Available online at www.eccomasproceedia.org
Eccomas Proceedia COMPDYN (2023) 5155-5178

ECCOMAS
Proceedia

COMPDYN 2023
9th ECCOMAS Thematic Conference on
Computational Methods in Structural Dynamics and Earthquake Engineering
M. Papadrakakis, M. Fragiadakis (eds.)
Athens, Greece, 12-14 June 2023

EFFECT OF DEBONDING ON GUIDED WAVE PROPAGATION IN STIFFENED COMPOSITE PLATE UNDER OPERATIONAL LOADING AND HYGROTHERMAL ENVIRONMENT

Akshay Prakash Kalgutkar[1], and Sauvik Banerjee[2]

[1] Research scholar, Department of Civil Engineering,
Indian Institute of Technology Bombay, Mumbai, 400 076, India
e-mail: akshay_kalgutkar@iitb.ac.in

[2] Professor, Department of Civil Engineering,
Indian Institute of Technology Bombay, Mumbai, 400 076, India
e-mail: sauvik@civil.iitb.ac.in

Abstract

Composite stiffened panels are extensively used in a wide range of engineering structures. However, these structures are subjected to external environmental and operational loading conditions, which may cause damage such as interlayer delamination or skin-stiffener interfacial debonding due to the development of enormous stresses. As a result, monitoring the induced hidden flaws and discontinuities in these structures becomes critical. Ultrasonic-guided wave techniques exhibit an efficient and accurate approach for monitoring discontinuities or damages in composite structures. The current study proposes a multiphysics numerical simulation using commercially available finite element software COMSOL Multiphysics to study guided wave propagation in a stiffened composite plate debonded at the plate-stiffener interface with a piezoelectric transducer subjected to in-plane mechanical load and hygrothermal environment. The plate and PZT patch are modelled using the brick element, and the debond is simulated using a through-width groove of 0.1 mm depth in the attached stiffener. A detailed parametric investigation considers the variations in debonding size, in-plane load and hygrothermal load intensity. The results show that the magnitude of the A0 mode is high in the bonded panel, whereas the S0 mode amplitude is low. In contrary, the scattered wave shows high S0 mode amplitude and a relatively low A0 mode amplitude in the debonded panel. Furthermore, as the magnitude of the compressive edge load increases, the group velocity of the A0 mode decreases, whereas, the group velocity of the S0 mode doesn't change significantly. Also, the size of time interval of the A0 mode packet and its amplitude reduce with the rise in the moisture concentration.

Keywords: Debonded stiffened composite panel, guided wave, in-plane edge load, hygrothermal load, COMSOL Multiphysics, piezoelectric patches.

ISSN:2623-3347
Peer-review under responsibility of the organizing committee of COMPDYN 2023.
doi: 10.7712/120123.10791.20417

1 INTRODUCTION

Thin-walled structures are usually supported on the stiffener to enhance the structural strength without significantly increasing to overall weight. However, the stiffened plate is vulnerable to damage such as fibre breakage, interlayer delamination or skin-stiffener debonding caused by the external in-plane load or extreme environmental conditions. Sometimes, these damages are not always detectable through visual inspection. These discontinuities may advance progressively, leading to catastrophic failure if not inspected and repaired in the early stage. It is observed that damage detection in the composite structure is more intricate when compared to the metallic forms due to its anisotropic [1, 2] and diverseness in the arrangement of plies. Therefore, it is imperative to evaluate the health of the composite material. Today, many nondestructive testing (NDT) methods are available that can easily detect and feature the surface and internal structural discontinuities without causing any damage. Some of them are ultrasonic C-scan [3], ultrasound wave distortion indicator [4], and laser ultrasonic [5], to name a few. These techniques are costly and time-consuming to use for inspecting large structures. On the other hand, monitoring damages or discontinuities in composite structures can be done efficiently and accurately using ultrasonic-guided wave (GW) methods. To develop infallible damage monitoring systems, it is necessary to have a thorough understanding of the quantitative characteristics of ultrasonic-guided waves that travel through composite laminates.

Lamb wave-based damage detection methods have been widely used to inspect thin structures [6]. The detection of debond [7-9] or low-velocity impact damage in stiffened composite panels [10] has been the subject of numerous numerical simulations and experiments using an actuator-sensor network. However, these techniques have difficulty dealing with general stiffened composite panels. Because of the multi-mode characteristics, dispersion, and direction dependence of the wave velocity, lamb wave propagation in composite plates is complicated [11]. Analyses can become more complex as a result of the addition of stiffeners. Finite element analysis and experiment were used by Guo and Cawley [12] to study the interaction of the S0 Lamb mode with delamination. The transmission and mode conversion of Lamb waves across adhesively bonded lap joints were investigated by Lowe et al. [13] employing finite element method (FEM).

Despite some progress, the knowledge of Lamb wave propagation in stiffened panels is still largely restricted to homogeneous and isotropic plates. To eliminate the direction dependence of the Lamb wave velocity, most researchers have concentrated on quasi-isotropic composite panels. Through FE simulations and experiments, Ramadas et al. [14] investigated the incident A0 mode interaction with a T-joint structural discontinuity in a composite structure. The authors noticed that a converted S0 mode is generated with the interaction of A0 mode with the junction. Han et al. [15] conducted a thorough investigation of the interaction between GW signals and structural discontinuity. The study demonstrated that when a signal propagates through a T- stiffener, a variety of modes are generated.

Chen and Wilcox [16] examine the effects of axial load on the guided wave characteristics. They showed that at low frequency-thickness values, the change in phase velocity caused by applied strain is nonlinear. Further, Lee et al. [17] demonstrated that a change in applied load primarily affects the time or phase of the scattered Lamb wave signals. In another study, Michaels et al. [18] looked into the effects of uniaxial loading on signals. The scatter signal's amplitudes were seen to rise monotonically as the load increases, but their shapes did not significantly alter. In order to account for changes in phase shifts and signal amplitude, Roy et al. [19] developed a load compensation model for ultrasonic-guided waves based structural

health monitoring (SHM). The literature shows that no study investigates the scattered wave response in the plate with debonding subjected to the external loading condition.

On the other hand, many researchers have examined the effects of temperature variations on Lamb wave propagation through experimentation. Generally, Lamb wave amplitude and arrival time are typically impacted by temperature variations [20]. In an experimental study, Boon et al. [21] showed that rising temperature reduces the group velocity of the wave. Later, to investigate the effects of changes in plate material properties on Lamb wave propagation due to temperature variations, Roy et al. [22] conducted the parametric studies using numerical wave propagation simulations. To understand the behaviour of Lamb modes due to change in ambient temperature, Sikdar et al. [23] performed a combined theoretical analysis, time-domain spectral element simulation and experimental analysis of elastic wave propagation in a carbon-fibre reinforced adhesively-bonded composite structure. Dan et al. [24] introduced the Equivalent Wave method (EWM) for developing new Rayleigh-Lamb equations with temperature-dependent variables. Without prior knowledge of the temperature dependencies of the material properties, EWM facilitates the prediction of the Lamb wave behaviour with temperature. Few studies have been done to investigate the impact of moisture concentration on the scattered wave response, aside from the analysis of the wave response under the influence of temperature. The effect of moisture absorption on the propagation of Lamb waves in viscoelastic composite materials was studied by Schubert and Herrmann [25]. They have demonstrated that moisture absorption results in a significant decrease in the sensor response's amplitude, which is linked to both changes in the material's and the adhesive layer's properties, and a relatively minor decrease in Lamb wave velocity in composite materials.

From the review, only few numerical techniques have been developed to simulate the hygral effect on the scattered wave response. Recently, a good amount of research has been carried out on the guided wave response in the panel under in-plane edge or operational loading conditions. However, as evidenced by the preceding literature, only a few works have considered GW response study in the panel debonding between the skin and stiffener interface. It becomes practically essential to consider the effect of the environmental condition and external loading on analysing the wave response in the plate with plate-stiffener interfacial debonding, which remains unexplored and inadequately represented.

The current investigation deals with the influence of environmental effect and loading effect on the GW response of the interfacial debonded stiffened panel while taking into account the residual stress generated due to hygrothermal load and in-plane load. A numerical study is conducted using FE simulation software "COMSOL Multiphysics". The current model considers two critical mechanisms coupled to each other to investigate the influence of in-plane edge load and hygrothermal load on GW propagation. A through-width groove of 0.1 mm depth is added to the lower surface of the stiffener to simulate debonding in the model. Furthermore, a preliminary non-linear numerical analysis is carried out to consider the impact of loading. The investigation is carried out in two stages. To start, a static analysis is performed to determine the stress that is induced due to mechanical and hygrothermal loading. The stress developed in the static study is employed as the initial condition to carry out guided wave investigation, which is a time-dependent investigation that employs an implicit time-step analysis. A detailed parametric investigation is carried out by considering the variations in debonding size, in-plane load and hygrothermal load intensity on the behaviour of the guided wave using different wave features.

2 MODELLING APPROACH IN THE COMSOL MULTIPHYSICS

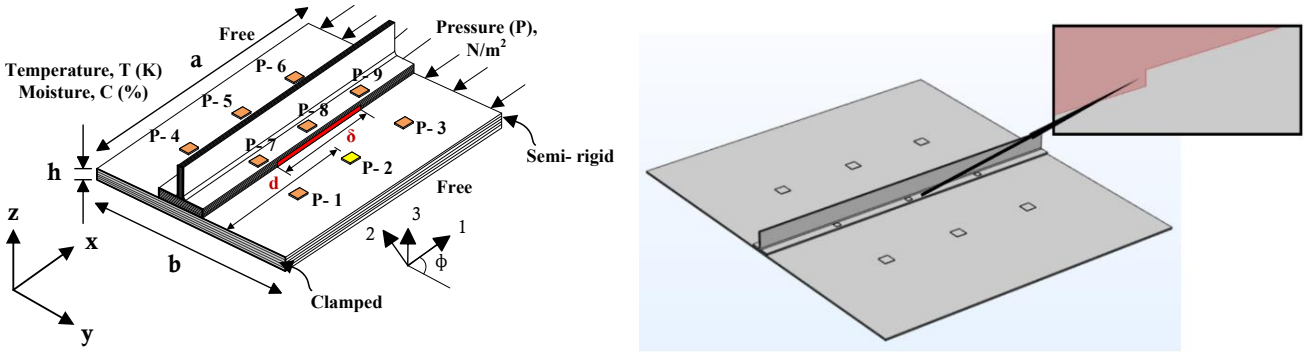

(a) (b)

Figure 1: (a) Model of stiffened panel attached with the piezoelectric patches, (b) Debonded stiffened panel modelling in COMSOL.

This study aims to investigate the wave propagation behaviour in a T-stiffened composite plate with interfacial debonding attached with PZT patches using finite element modelling. The finite element analysis (FEA) is completed with the software package COMSOL Multiphysics version 5.5. The current study is conducted on the T-stiffened panel that is debonded at the plate-stiffener interface and exposed to external environmental and in-plane loading. The panel has a dimension of a, b, and h in the x, y, and directions, respectively. The T stiffener is attached on the top surface of the panel, which has a flange of $b_f \times t_f$ and a web of $t_w \times d_w$. The panel is exposed to the non-mechanical load of temperature 'T' and moisture 'C', as shown in Fig. 1 (a). This section overviews the settings and initial setup of COMSOL employed for this research. The current study considers the solid mechanics and electrostatics modules coupled with piezoelectric effect multiphysics. Finally, the two steps studies are carried out with an initial stationary study to carry out the stress analysis due to in-plane load or hygrothermal load, followed by the time-dependent study to simulate the wave propagation study in the stressed plate.

2.1 Physics of simulation

The physics of simulating GW in the stiffened composite panel under load conditions or hygrothermal environment is simplified and shown in Fig. 1 (a). A stiffened plate is loaded at one end and fixed on the other end. Nine piezoelectric sensors (PZT 1 to PZT 9) are mounted on the plate and stiffened flange surface, as shown in Fig. 1(a). The current study ignores the adhesive layer because the load introduce has little influence on it [26]. As a result, one simulation model should integrate the acoustoelastic effect, piezoelectric effect, and loading influence on piezoelectric sensors. In addition, the static load is considered. Thus, the GW excitation and response process must be simulated under static load conditions. Considering the above-discussed physics, the multiphysics module called the Piezoelectric effect is adopted, as shown in Fig. 2. The mechanics features of the stiffened composite plate and the piezoelectric sensors are simulated using solid mechanics physics, while the electric features of the piezoelectric sensors are simulated using electrostatics physics. However, these two physics are coupled by the Multiphysics-Piezoelectric Effect. The details of the steps carried out in each physics of the simulation are explained elaborately as follows:

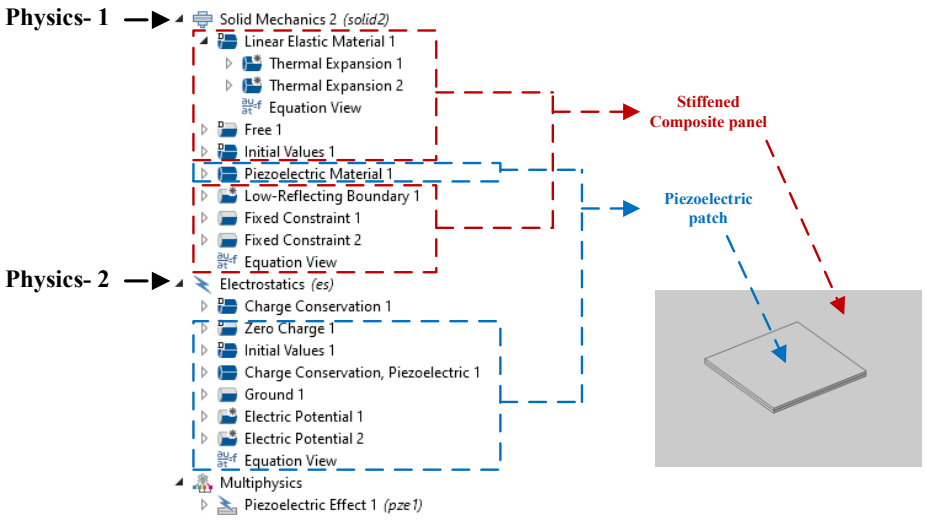

Figure 2: The simulation physics in COMSOL of GW propagation under thermal condition

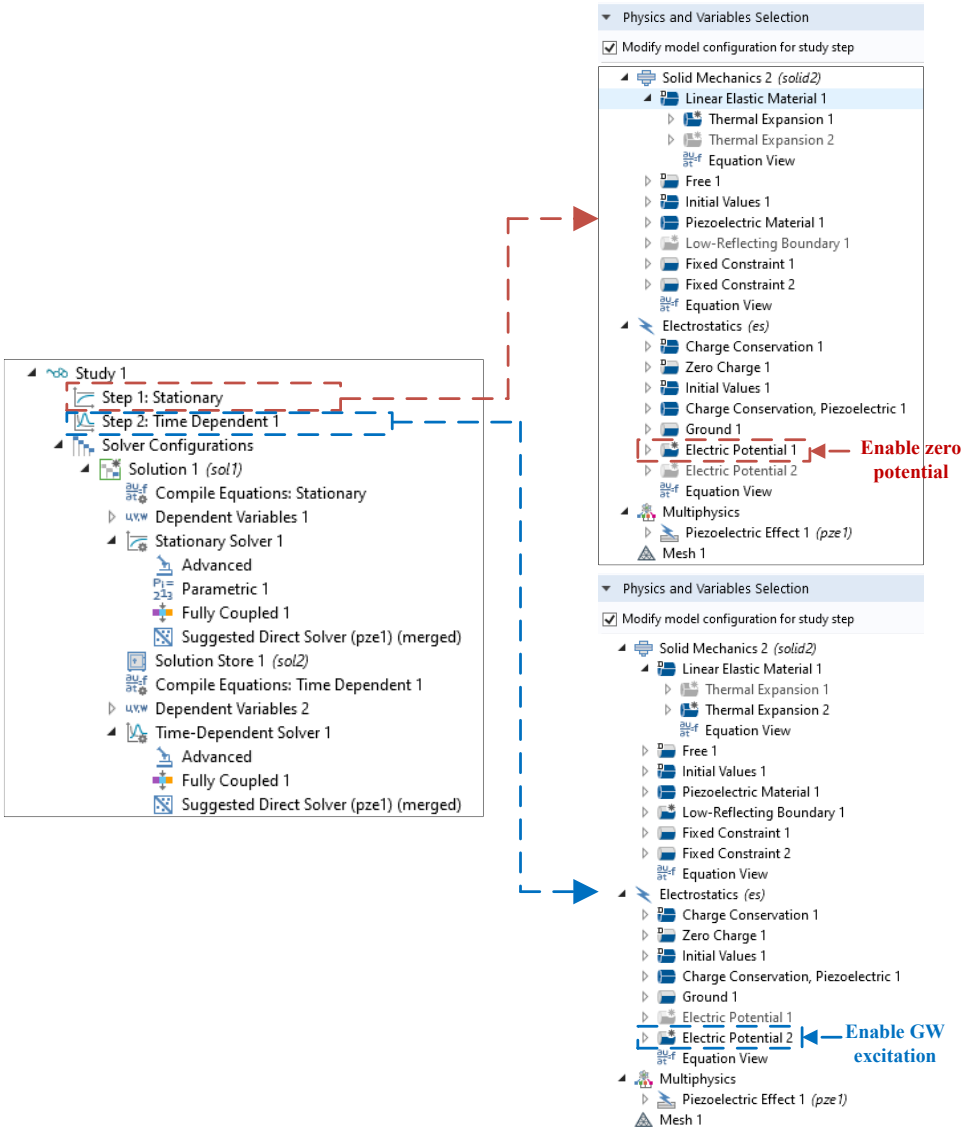

Figure 3: The solver settings of the Multiphysics simulation model.

Solid Mechanics:

- Initially, the material behaviour with the properties for the stiffened panel and the piezoelectric patches are assigned using the linear elastic material and piezoelectric material options, respectively.
- The Fixed Constraints and Prescribed Displacement options are used to simulate boundary conditions, while the Boundary Load option is used to apply an external in-plane load to the plate.
- Similarly, the hygrothermal load is applied as the lumped mass using the thermal expansion and hygroscopic swelling option under the linear elastic material model.
- Furthermore, the opposite edges of the stiffened plate are constraints such that in-plane is not allowed. As the current investigation is carried out using two studies, the load, regardless of the external in-plane load or hygrothermal load, is applied as the two loading options. In the static study, the load is applied incrementally to converge the results well. Further, the load is directly applied in one step so that the applied load is maintained constant during the time-dependent step.
- Low-Reflecting Boundary is employed to reduce the boundary edge reflection of GW. The damping type is set to be "User defined", with the mechanical impendence set to density times the average of P and S waves velocities.
- Piezoelectric material combined with Electrostatics is employed to simulate the piezoelectric sensors.

Electrostatics:

- This physics, along with the piezoelectric material option, is employed to the geometry that is used as the piezoelectric sensors.
- The lower surface of all the piezoelectric sensors are grounded to zero electric potential using the Ground option.
- Similar to the loading, electric potential is applied in two devises, Electric Potential 1 and Electric Potential 2, which are set to zero potential and a voltage waveform of the GW excitation, respectively. They are applied on the upper surface of the piezoelectric patch that is used as an exciter. However, there are mutually exclusive in the subsequent studies, which will be explained in section 2.2.

Further, the elastic properties of the piezoelectric patches are coupled with the electrical properties with the use of the Piezoelectric Effect option in the Multiphysics module.

2.2 Study solver of simulation

The current study considers two study steps for solving the considered multiphysics model, as shown in Fig. 3. The first step is carrying out the stress analysis using the stationary study. The load is employed incrementally to improve the convergence of the result. Further, the results of the stationary study are used as the initial value of the time-dependent study, which simulates the process of GW excitation-propagation-response under the loading condition.

Fig. 3 presents the physics setting for each study step. In the stationary study, zero voltage is applied on the surface of the actuator patches. This directly shows that Electric Potential 1 of zero potential is enabled, but Electric Potential 2 of GW excitation is disabled. This is carried out to avoid the generation of the DC bias voltage, which would introduce the stress caused due to the load. However, if the DC bias voltage is induced, it would be a step excitation in the time-dependent study initiating a wideband GW propagating on the stiffened plate leading to a false GW response signal output from receiver PZTs [27]. Further, it is observed that

when the stress induced in the plate is high, the receiver PZT produces a false output signal due to improper convergence of the result of Step 1. Further, load ramping is performed using an auxiliary sweep technique, in which the load is applied incrementally to improve convergence. In the time-dependent step, Electric Potential 1 is disabled, and Electric Potential 2 is enabled for GW excitation. Thus, the GW signals for different parametric conditions can be obtained. Guided wave simulation is carried out by employing a generalised alpha method time stepping method with a constant time step of 5×10^{-8} s.

3 PROBLEM DESCRIPTION AND SIGNAL PROCESSING TECHNIQUES

3.1 Problem definition

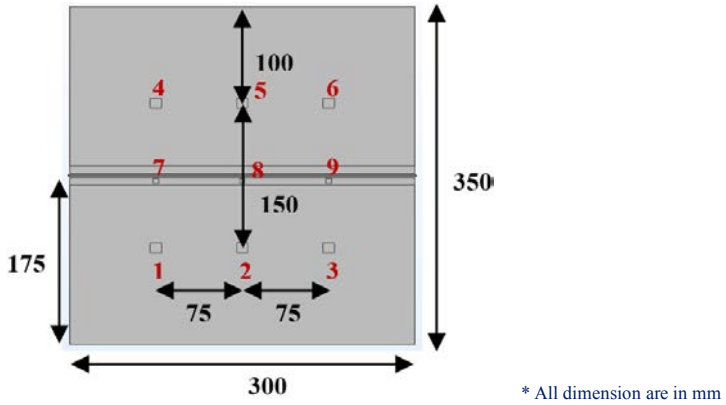

Figure 4: Arrangement of PZT patches on the surface of stiffened composite panel.

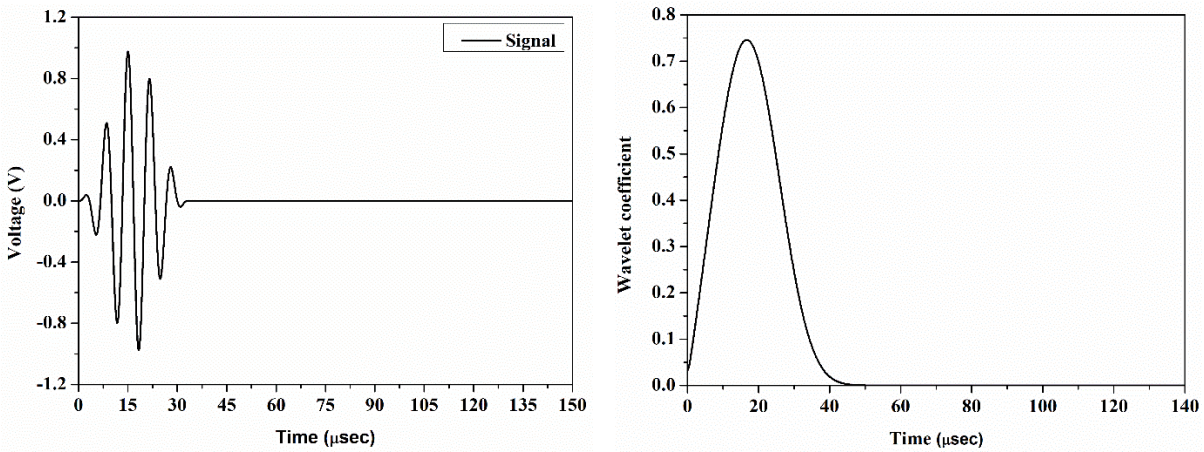

(a) (b)

Figure 5: 5-cycle Hanning window response excited at 150 kHz and (b) Wavelet of the response at 150 kHz frequency.

The investigation is conducted on the stiffened composite panel with the 0^o ply orientation, i.e., fibres along the length of the attached stiffener. The plate with length, a= 300 mm, breadth, b= 350 mm and thickness, h= 2 mm, is considered, which is exposed to the non-mechanical load with a reference temperature of 300 K and reference moisture of 0.0 %. In this investigation, the centrally placed T-stiffener is considered with the width of the flange b_f of 20 mm, and thickness t_f is considered to be 2 mm, whereas the depth d_s and width b_s of the web are 18 mm and 2 mm, respectively. The debond of length 'δ' is introduced at the inter-

face of the stiffener and plate at the distance of 'd' from the clamped edge. The investigation considers nine piezoelectric patches from P-1 to P-9, with the centre to centre distance of 75 mm along the length and 150 mm along the plate's width between P1 to P-9 PZT, as shown in Fig. 4. Piezoelectric patches of P-7 to P-9 are attached to the surface of the stiffener flange, having a size of 5 mm x 5 mm with a thickness of 0.4 mm. The size of PZT P1 to P6, which are attached to the plate, has dimensions of 10 mm x 10 mm and a thickness of 0.4 mm. In the current study, the PZT- 2 is used as the actuator through which the 5-cycle sine pulse modulated with Hanning window, shown in Fig. 5, is employed as the input pulse, with all of the other PZTs acting as receivers to obtain the scattered wave in the structure. Hanning pulse is defined as:

$$F(t)= 0.5\times (1-\cos(2\times\pi\times f\times t/N)) \times\sin(2\times\pi\times f\times t) \quad (1)$$

The panel under consideration is clamped at one end and semi-rigid conditions on the other. In the case of the semi-rigid condition, the edge (i.e., x= a) is restrained in all the transverse and rotational directions but free to move in the in-plane loading direction. Furthermore, the panel is maintained free on the edge parallel to the stiffener position (i.e., y= 0 and y=b), as shown in Fig. 1(a). To reduce the boundary edge reflection of the scattered wave, Low-Reflecting Boundary is employed with damping set to "User defined", with the mechanical impendence set to density times the average of P and S waves velocities.

3.2 Structural meshing

The current study employs a physics-controlled Tetrahedral mesh, with the mesh size determined by the wavelength of GW. Based on the literature [8], the Courant-Friedrichs-Lewy (CFL) convergence conditions suggest that the widest mesh be less than 1/6 of the wavelength of the wave modes. For instance, when the Hanning pulse is excited with 150 kHz in a 2 mm thick composite plate, the wavelength of S0 mode is nearly 14.9 mm, and the wavelength of A0 mode is found to be 6.78 mm from the dispersion curve for 0^o laminated plate shown in Fig. 7. Further from the Courant-Friedrichs-Lewy criteria, the mesh size should be less than 1.13 mm, leading to high computational cost. For the piezoelectric sensors, the smallest mesh size is set to be 1 mm. The complete mesh consists of 1420637 domain elements, 653315 boundary elements, and 10833 edge elements with 3353355 degrees of freedom.

Courant–Friedrichs–Lewy condition

Mesh and time step Criteria:

The CFL condition becomes

$$C = \frac{u_x \Delta t}{\Delta x} + \frac{u_y \Delta t}{\Delta y} \le 1 \quad \text{and} \quad \Delta x \le \frac{u_x}{6f}, \quad \Delta y \le \frac{u_y}{6f} \quad (2)$$

where the dimensionless number C is called the Courant number,

- u_x and u_y is the magnitude of the velocity in the x and y-axis. (whose dimension is length/time)
- Δt is the time step (whose dimension is time)
- Δx and Δy is the length interval (whose dimension is length).

3.3 Material properties

Table 1: Elastic moduli of carbon/epoxy at various temperatures; $G_{13} = G_{12}$, $G_{23} = 0.4G_{12}$, $\upsilon_{12} = 0.3$, $\alpha_1 = -0.3\times10^{-6}$/K and $\alpha_2 = 28.1\times10^{-6}$/K. C= 0.0 %

Elastic Moduli	**Temperature T (K)**					
(GPa)	300	325	350	375	400	425
E_1	172.5	172.5	172.5	172.5	172.5	172.5
E_2	6.9	6.17	5.81	5.45	5.08	4.9
G_{12}	3.45	3.45	3.16	2.88	2.73	2.59

The present investigation mainly focuses on the wave propagation response of a debonded stiffened composite panel under the influence of in-plane edge load and hygrothermal conditions. The material properties of the composite laminated panel and stiffener cases considered in this study are presented in Tables 1 and 2 for different temperatures and moisture concentrations. These properties have been referred from Parhi et al. [28] work.

Table 2: Elastic moduli of carbon/epoxy at various moisture concentrations; $G_{13} = G_{12}$, $G_{23} = 0.4G_{12}$, $\upsilon_{12} = 0.3$, $\beta_1 = 0$ and $\beta_2 = 0.44$. T= 300 K

Elastic Moduli	**Moisture Concentration, C%**					
(GPa)	0.25	0.50	0.75	1.00	1.25	1.50
E_1	172.5	172.5	172.5	172.5	172.5	172.5
E_2	6.72	6.54	6.36	6.17	6.17	6.17
G_{12}	3.45	3.45	3.45	3.45	3.45	3.45

Table 3: Material property of piezoelectric sensor (PZT-5A) under loading condition.

Parameter		**Values**
Relative permittivity	ε_{11}	1730
	ε_{33}	1700
Piezoelectric constant ($\times10^{-10}$ C/N)	$d_{31}= d_{32}$	$-1.71-1.71\times (0.1328.e^{0.0022.\sigma} - 0.1328.e^{-0.0476.\sigma})$
	d_{33}	3.74
	d_{15}	5.84
Compliance coefficient ($\times10^{-12}$ m^2/N)	sE_{11}	16.4
	sE_{12}	-5.74
	sE_{13}	-7.22
	sE_{33}	18.8
	sE_{55}	4.75
	sE_{66}	4.43
Density (kg/m3)	ρ	7750
Elastic properties (GPa)	$E_{11}= E_{22}$	60.97
	E_{33}	53.19
Poison ratio	$\upsilon_{13}= \upsilon_{23}$	0.4402
	υ_{12}	0.35

Similar to the degradation of the elastic properties of the composite material, the external load change the piezoelectric material's electrical properties. Table 3 shows the material properties of the piezoelectric sensors PZT-5A as a function of loading. It is observed that only the d_{31} parameter is varied when the plate is under the action of external load, and an em-

pirical relation referred from the work of Qiu et al. [27] is employed in which σ is the applied pressure in MPa.

Table 4: Material property of piezoelectric sensor (PZT-5A) under elevated temperature.

Parameter		At T= 300 K	Elevated temperature (ΔT= T-273), K
Density (kg/m^3)	ρ	7750	$7751.80 - 7.26e^{-02}\Delta T$
Elastic properties	$E_{11}= E_{22}$	60.97	$60.45 + 2.09e^{-02}\Delta T$
(GPa)	E33	53.19	$52.95 + 9.8e^{-03}\Delta T$
	$\nu_{13}= \nu_{23}$	0.4402	$0.43 + 3e^{-04}\Delta T - 3e^{-06}(\Delta T)^2 – 1e^{-09}(\Delta T)^3$
Poison ratio	ν_{12}	0.35	$0.35 + 2e^{-04}\Delta T - 8e^{-07}(\Delta T)^2 + 2e^{-09}(\Delta T)^3$
	$d_{31}= d_{32}$	-171	$170.78 – 7.1e^{-03}\Delta T+6e^{-04}(\Delta T)^2 + 2e^{-16}(\Delta T)^3$
Piezoelectric constant	d_{33}	374	$369.12 +1.49e^{-01}\Delta T+1.9e^{-03}(\Delta T)^2-4e\text{-}^{09}(\Delta T)^3$
(×10^{-12} C/N)	d_{15}	584	584

Further, thermal load has an impact on both the piezoelectric material's electrical and elastic properties and are shown in Table 4. The density, elastic properties and piezoelectric parameters are varied for different intensities of temperature. Further, for obtaining the value of the different material constant, an empirical relation referred from the work of Roy et al. [22] is employed, where ΔT is the elevated temperature from 273 K temperature. However, no existing literature on the influence of moisture on piezoelectric properties is available. Hence, the piezoelectric constant at the reference temperature of 300 K is used for the elevated moisture concentration, and only the elastic properties of the composite material are varied, as presented in Table 2.

3.4 Signal processing techniques

The characteristics of guided waves have been thoroughly investigated using conventional non-destructive evaluation, making them an intriguing technique for inspecting intricate structures. Inspection of complex structures is difficult due to the generation of new modes or the reflections from overlapping features. Therefore, determining the number and amplitude of the wave packets present in ultrasonic time traces is essential for creating a robust guided wave inspection system that can identify changes in the measured signal over time caused on by particular parameters. To resolve closely spaced events and distinguish the parametric changes caused by structural features, an appropriate and reliable signal processing tool for structural health monitoring is therefore required. Hence, in the current investigation, the peak of the wave modes and Continous wavelet coefficient (CWT) along with the correlation coefficient of the response are used as a tool for measuring the wave features.
The continuous wavelet transform is defined as follows

$$CWT_x^{\psi}(\tau,s) = \Psi_x^{\psi}(\tau,s) = \frac{1}{\sqrt{|s|}}\int x(t)\ \psi^*\left(\frac{t-\tau}{s}\right)dt \tag{3}$$

where s and τ is the scaling and the translation parameters, respectively. ψ(t) is the transforming function, and it is called the mother wavelet.

Further, the Correlation Coefficient is used to compare the signal from the various parameters with a signal of the bonded plate subjected to no loading conditions. The correlation coefficient of two random variables is defined as

$$\rho(A,B) = \frac{1}{N-1}\sum_{i=1}^{N}\left(\frac{A_i - \mu_A}{\sigma_A}\right)\left(\frac{B_i - \mu_B}{\sigma_B}\right) \tag{4}$$

where μ_A and σ_A are the mean and standard deviation of signal A, respectively, and μ_B and σ_B are the mean and standard deviation of response B.

4 RESULTS AND DISCUSSION

This section discusses the theoretical investigation of the scattered guided wave response characteristics in debonded stiffened panels subjected to in-plane edge loading and hygrothermal environment using COMSOL Multiphysics. In order to comprehend the effects of in-plane loading and hygrothermal conditions on the structure, the scattered wave response in the stiffened plate is investigated in this work. Various signal processing techniques are used to investigate the signal's features.

4.1 Validation study of the wave response

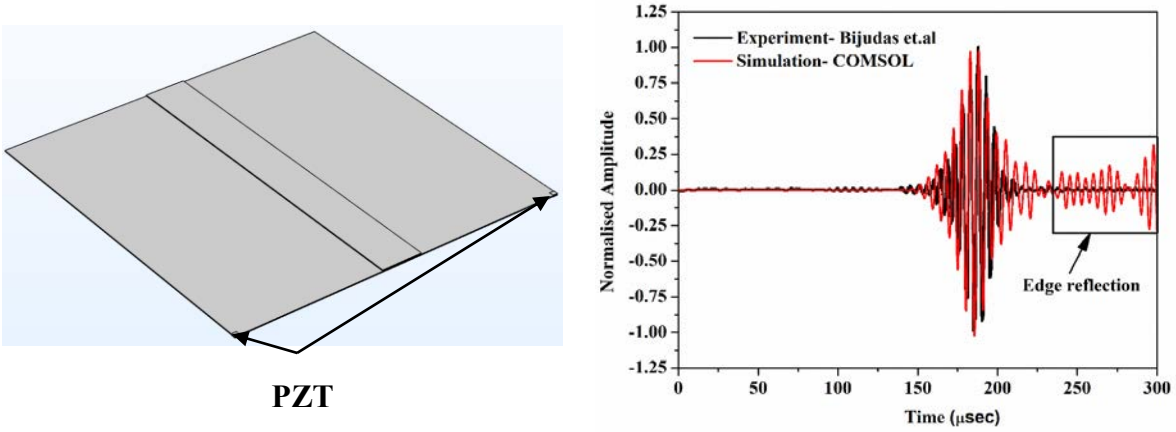

(a) (b)

Figure 6: (a) current COMSOL Multiphysics model, (b) Validation study of the wave response in the stiffened aluminum panel.

To carry out any numerical simulation, it is necessary to validate the outcomes of the developed model against the response of the existing available literature. In the current work, the guided wave response of the spread-stiffened panel obtained from the current simulation is compared with the experimental results of Bijudas et al. [29]. The experiment is carried out on an aluminum-stiffened panel with a spread stiffener attached across its width at the centre of the panel. The PZT patches are attached to the top and bottom surfaces of the panel in order to generate a specific wave mode by adjusting the polarity of the actuating signal. A square piezoelectric patch is attached at the one corner of the panel, and the response is captured using top and bottom bonded PZT on the other end corner. The study is conducted by exciting the 8-cycle Hanning window at 200 kHz. The current study response is plotted against the exist-

ing work response in Fig. 6 (b). To compare the two signals, the response is normalised using the min-max normalisation method. The results show that the first wave packet from 150 µsec to 220 µsec closely matches each other. However, a wave packet due to edge reflection is observed after 225 µsec. This is due to the attachment of receiver PZT at other edges of the simulated panel, which is not the case in the experiment setup, as the PZT is attached far from the edge to avoid reflection. As a result, the current model can be used to carry out parametric investigations considering the effect of in-plane edge and hygrothermal conditions.

4.2 Effect of excitation frequency on the amplitude of the scattered wave

Prior to conducting the parametric study with guided wave, it is essential to identify the various wave modes generated in the structure. To understand the behaviour of the various modes, a slowness curve is initially plotted using the semi-analytical finite element (SAFE) method [30] at 150 kHz frequency, as presented in Fig. 7 (a) to understand the variation of velocity of wave modes in different propagating direction. This study is required due to the anisotropic behaviour of the composite material. The plot shows that the wave propagates with maximum velocity along the fibre direction and gradually drops when the wave travels normal to the fibre direction. Further, the dispersion curve is plotted as shown in Fig. 7 (b) by considering the wave propagating normal to the fibre length to identify the wave modes based on the group velocity for different excitation frequencies.

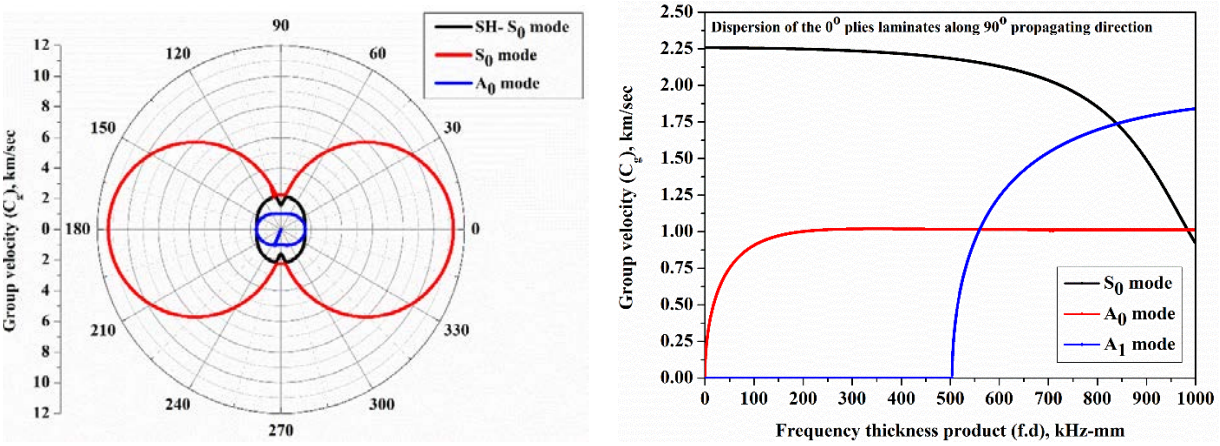

(a) (b)

Figure 7: (a) Slowness curve of the 2 mm panel at 150 kHz excitation frequency (b) Dispersion curve of the 0° laminated panel along 90° propagating direction.

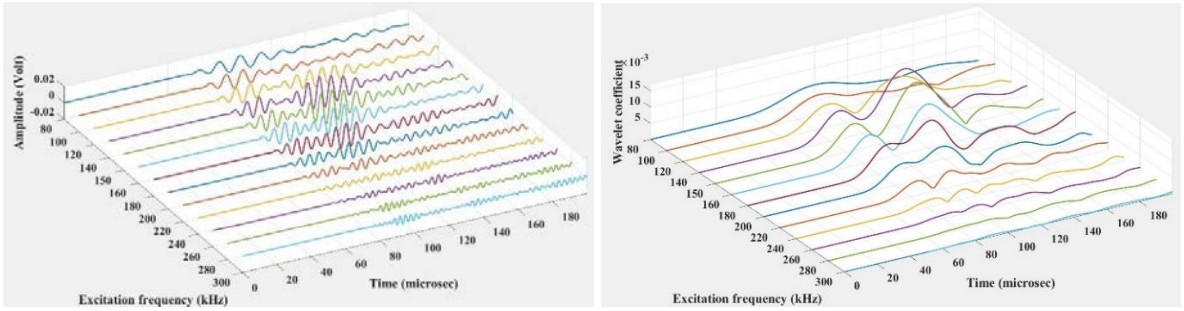

(a) (b)

Figure 8: Wave response and the wavelet plot for different excitation frequencies.

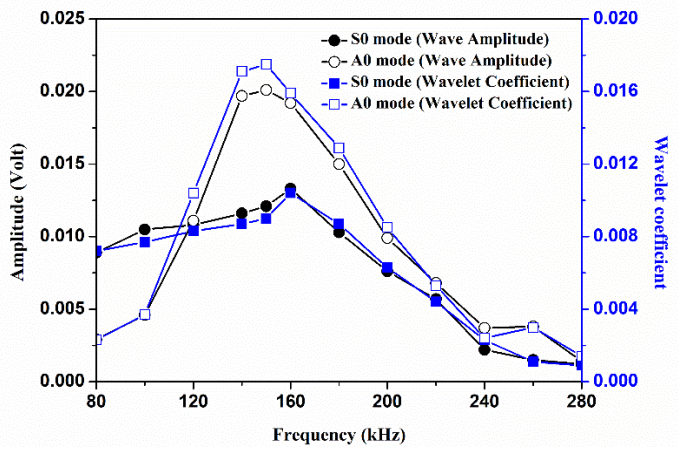

Figure 9: Frequency modulation curve of the 0° T-stiffened composite panel.

Subsequently, in this section, the frequency-amplitude modulation curve is plotted to understand the effect of excitation frequency on the amplitude of S0 and A0 modes. The current investigation is conducted on the bonded rectangular composite stiffened panel with 0° orientated laminates. The 5-cycle Hanning window is used in the study, with the excitation frequency varied from 80 kHz to 280 kHz, and the corresponding peak amplitude and wavelet coefficient of the two fundamental modes (A0 and S0) are recorded. The wave is excited in the panel using the P2 patch, and the response is captured at the P5 patch, such that the exciter and the receiver PZTs are positioned collinearly. Fig. 8 depicts the wave response and the wavelet plot at the corresponding excitation frequency. The frequency modulation curve of the current study is presented in Fig. 9. The obtained response shows that with the rise in the excitation frequency upto 150 kHz, the peak amplitude and wavelet coefficient of A0 mode initially increases, and a further increase in the excitation frequency reduces the signal's amplitude. However, the amplitude and wavelet coefficient of the S0 mode increases upto 160 kHz, and then a drop is noticed with the rise in the signal excitation frequency. Hence, this shows that both the modes have a significant effect when excited at the frequency close to 150 kHz and in the further parametric study, the plate is excited with a 5-cycles Hanning pulse at the 150 kHz frequency using PZT patch P2 unless otherwise specified.

4.3 Parametric investigation to understand the effect on the guided wave response

This section investigates the influence of different parameters like debond size, inplane edge load intensity and hygrothermal condition on the scattered wave response in the panel. The study is conducted on the rectangular panel provided with the T-stiffened at the centre. In the current study, the edges at which the stiffened is connected are rigidly held, and the other two edges are freely supported unless the in-plane load is applied. In the case of in-plane load, the non-loaded edge is rigidly connected, while the other edge is made semi-rigid, allowing the plate to move in the loading direction. The current investigation uses 8 PZTs to capture the structure's wave response, with P2 acting as the actuator. In the study, a 5-cycles Hanning window is excited at a frequency of 150 kHz as it significantly influences the wave modes amplitude, as noticed in the previous study. Furthermore, various signal processing techniques, such as CWT peak and correlation coefficient, are used to understand the wave's features under different parametric variations.

4.3.1 Effect of debonding size on the scattered GW response

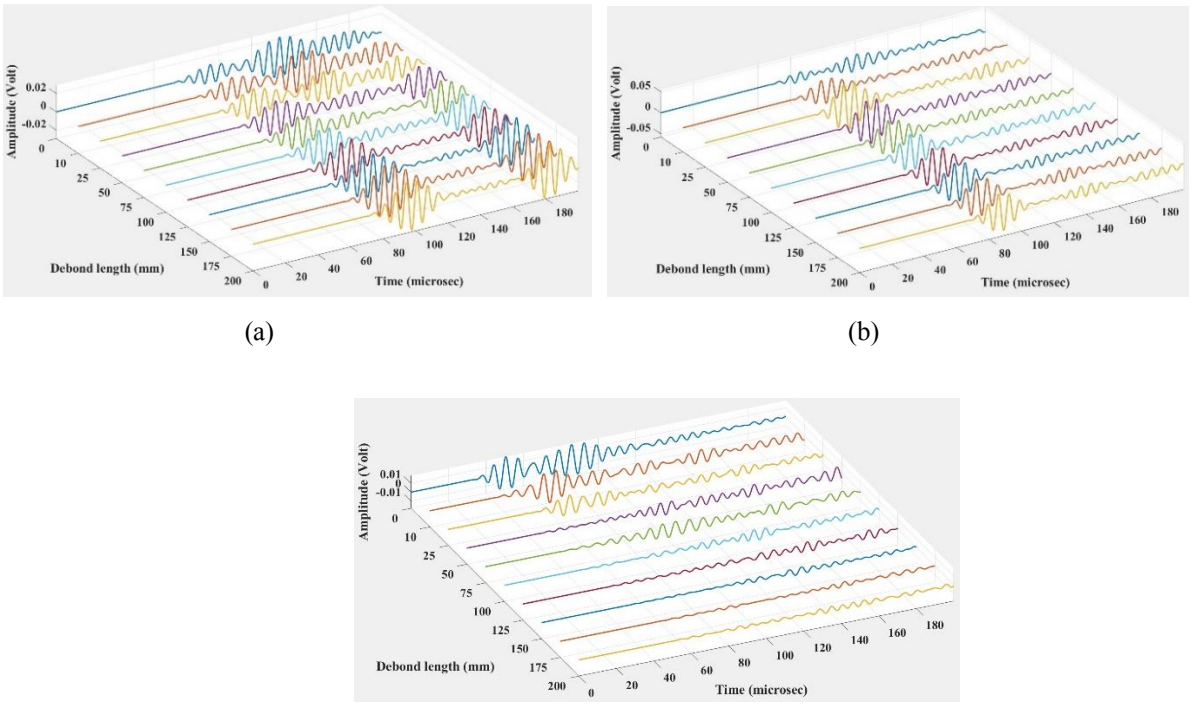

Figure 10: Variation of response for different debonding lengths captured at (a) P4, (b) P5 and (c) P8.

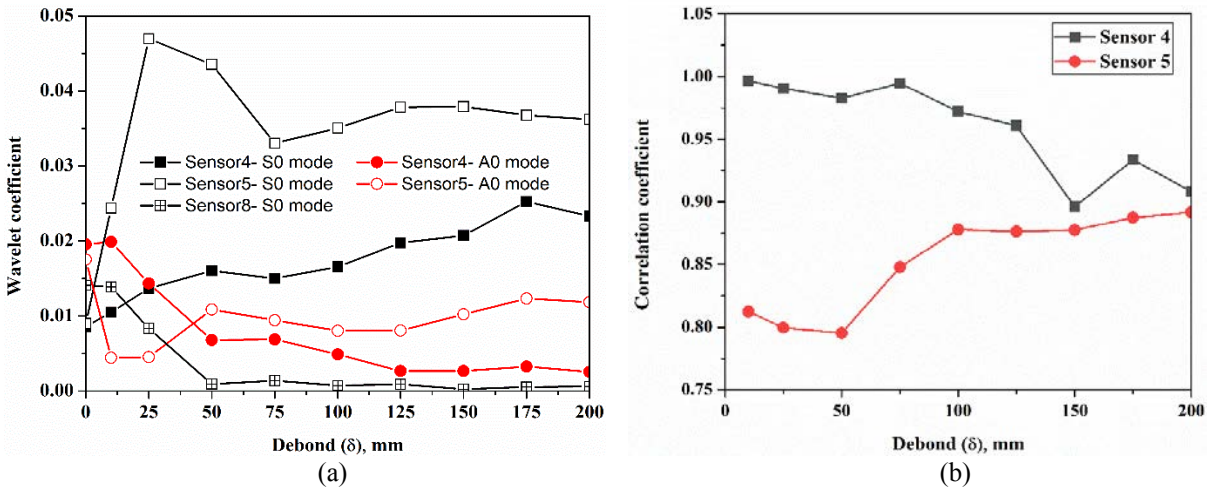

Figure 11: Variation of the (a) wavelet coefficient and (b) correlation coefficient of the wave response for different debonding sizes.

This section provides insight into debonding size impact on the scattered wave response. The current study uses the rectangular stiffened panel to understand the wave response. The investigation is carried out by introducing the debond between the plate and the stiffener in the central region of the panel. The debond is introduced by creating a grove of 0.1 mm depth over a stiffener flange surface so that the plate and stiffener do not come into contact. Also, this will avoid the contact non-linearity developed during the loading time, which increases the computational cost. However, with this type of modelling, the boundary reflection may be captured in the response from the edge of the groove. Fig. 10 shows the wave response in the

panel due to different debonding sizes captured at various PZTs. Fig. 11 (a) shows the wave response that is captured at P4, P5 and P8, and it is observed that the amplitude of the S0 mode of the signal captured through P4 enhances tremendously as the size of debonding increases. However, as the size of the debonding increases, the amplitude of the A0 mode decreases. Similar behaviour is observed in the response captured at the P5 patch, where the peak of the A0 mode wavelet coefficient drops initially with the introduction of debond and then increases marginally with the enhancement in the debond size. On the other hand, the signal captured by the patch P8 attached to the surface of the stiffener shows a reduction in the S0 mode wave amplitude due to debonding. The behaviour of this mode is due to the increase in the signal travel path caused by an increase in the debond size, as the stiffener is not in contact with the panel.

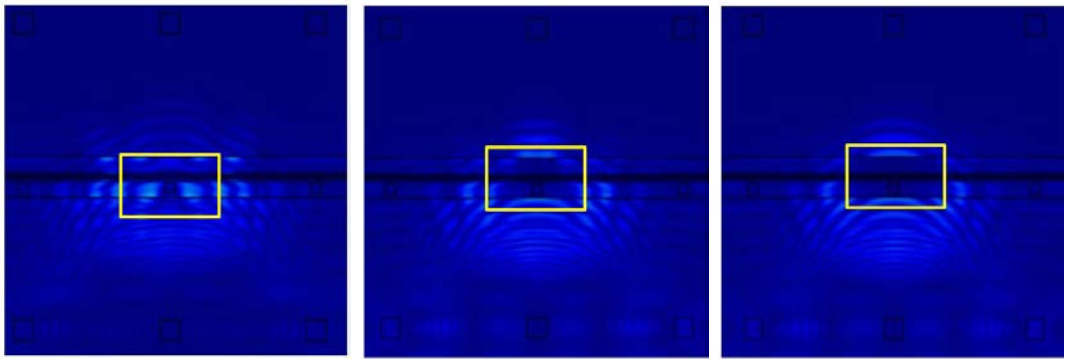

(a) (b) (c)

Figure 12: Top view of the displacement profile of the response around the attached stiffener in the panel provided with (a) δ= 0mm (b) δ= 25mm (c) δ= 50mm.

Further, to have a sight on the propagation of the wave across the debonded region in the stiffener, a displacement plot of the panel with centrally positioned debond of various length is shown in Fig. 12. It can be observed that in the case of the bonded plate, the wave propagates through the stiffener, which is shown by the wavy colour in the highlighted portion. This shows a greater amplitude of the first wave packet in Fig. 10 (c). However, as the debonding length increases, the wave propagates only through the plate in the debonded region, which is shown by a constant colour around the highlighted portion in the displacement plot. This demonstrates the reduction in the amplitude along with the delay in the propagating packet of the response captured by the P8 sensor, as shown in Fig. 10 (c).

The correlation coefficient of the S0 mode of the wave is established to understand the change in the wave response due to debonding, as presented in Fig. 11 (b). In the case of the P4 patch response, the similarity of the debonded condition signal to the bonded condition response decreases as the debonding length increases. However, in the case of the P5 patch response, the correlation coefficient reduces marginally with the initiation of debonding and then increases with the debonding size.

4.3.2 Effect of in-plane load on the scattered GW response for different debonding length

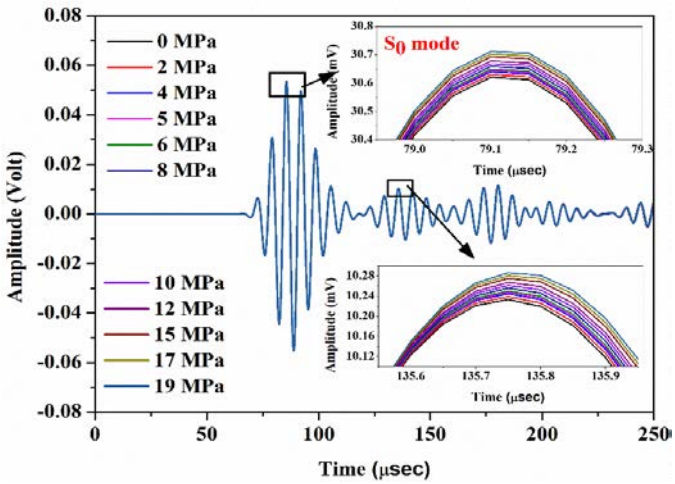

Figure 13: Wave response obtained at P5 sensor for δ= 25 mm.

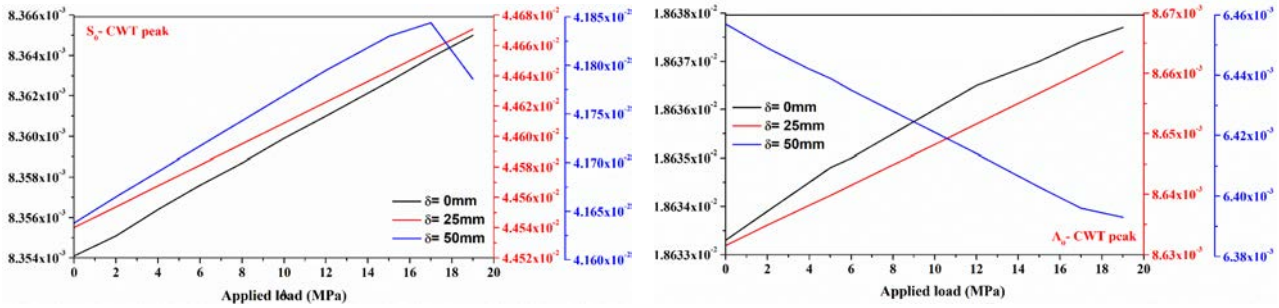

(a) (b)

Figure 14: Variation of the CWT peak of (a) S0 mode and (b) A0 mode obtained at P5 for different debond sizes.

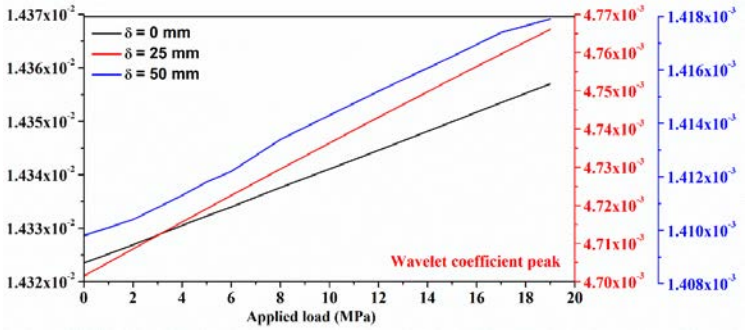

Figure 15: Influence of in-plane load on the CWT peak of the signal obtained at P8 for different debond length

The impact of the in-plane edge on the scattered guided wave response in an interfacial debonded stiffened composite plate is investigated in this section. The current investigation considers three contact conditions: no debond condition and centrally positioned debond of 25 mm and 50 mm centrally induced debond. The investigation is conducted by exciting a 5-cycles Hanning window through the P2 patch, and response is captured at the other eight piezoelectric patches. Compressive loading is applied in terms of pressure at the semi-rigid edge, while the opposite edge is rigidly held. According to the stability study, it is observed that the panel buckles at a pressure of 19.538 MPa, 19.523 MPa and 19.484 MPa for the bonded pan-

el, 25 mm debond panel, and 50 mm debond panel, respectively. Hence, in the current study, the load is applied from 0 to 19 MPa.

Fig. 13 shows the scattered wave response obtained at P5 for the case of the bonded stiffened panel. According to the study, the applied load has minimal effect on the wave response. Furthermore, as the intensity of the pressure increases, the wave amplitude increases marginally for both wave modes. Aside from the reduction in A0 mode amplitude, a slight delay in group velocity is observed. Fig. 14 (a) shows the CWT peak of the S0 mode for various debonding sizes. It demonstrates that the amplitude of the CWT peak rises as the intensity of the applied pressure increases. However, in the case of the 50 mm debonded panel, the peak of S0 mode CWT enhances, and then it starts to drop as the load approaches the buckling load. It can also be observed that the magnitude of the wavelet coefficient peak increases abruptly with the introduction of debonding and further drops, with an increase in the debonding size. However, in the case of the A0 mode wavelet peak, the rise in the magnitude of the peak is observed for the bonded panel and debond of 25 mm, as shown in Fig. 14 (b). Contrary, in the case of a 50 mm debond panel, the magnitude of the wavelet peak drops with the rise in the pressure intensity. Apart from this, the magnitude of the A0 mode CWT peak reduces with the enhancement in the debonding size.

Further, the P8 sensor response is studied using the CWT peak feature of the S0 mode (first packet) of the response for different debonding sizes. From Fig. 15, it is observed that the peak magnitude of the CWT increases with the enhancement in the applied load. However, the magnitude of CWT reduces as the size of debonding increases. This is due to the gap created in the stiffener representing the debond, which will increase the wave's travel path by damping the signal amplitude.

4.3.3 Effect of temperature on the scattered GW response for different debonding length

This section investigates the influence of temperature on the scattered wave response for various debonding sizes by maintaining the structure at a uniform temperature throughout the study. As discussed earlier, the temperature will degrade the composite material's elastic properties and the piezoelectric patch's elastic and electrical properties. As a result, temperature-dependent material properties are used in the study. Also, the stability study showed that the panel buckles at the temperature of 524.65 K, 524.42 K and 524.08 K for the bonded panel, 25 mm and 50 mm debonded panel, respectively. Therefore, the current investigation is carried out for the temperature ranging from 300 K to 425 K at an interval of 25 K. Fig. 16 shows the response of the wave captured through the P5 sensor for various temperature intensities and for different debonding lengths by considering a through-width debond of 20 mm. From the plot, it is noticed that in the case of a bonded panel, the amplitude of the A0 mode reduces significantly with the introduction of temperature. On the other hand, the amplitude of the S0 mode increases substantially with debonding, whereas the A0 mode will propagate with a much-diminished amplitude. Fig. 17 presents the CWT plot obtained at 150 kHz for the P5 patch response in a 25 mm debonded stiffened panel. The amplitude of the wavelet decreases initially and further increases with the rise in temperature. Along with this, there is a drop in the wave's group velocity as the intensity of temperature increases, evidenced by the shift in the wavelet peak towards the higher time.

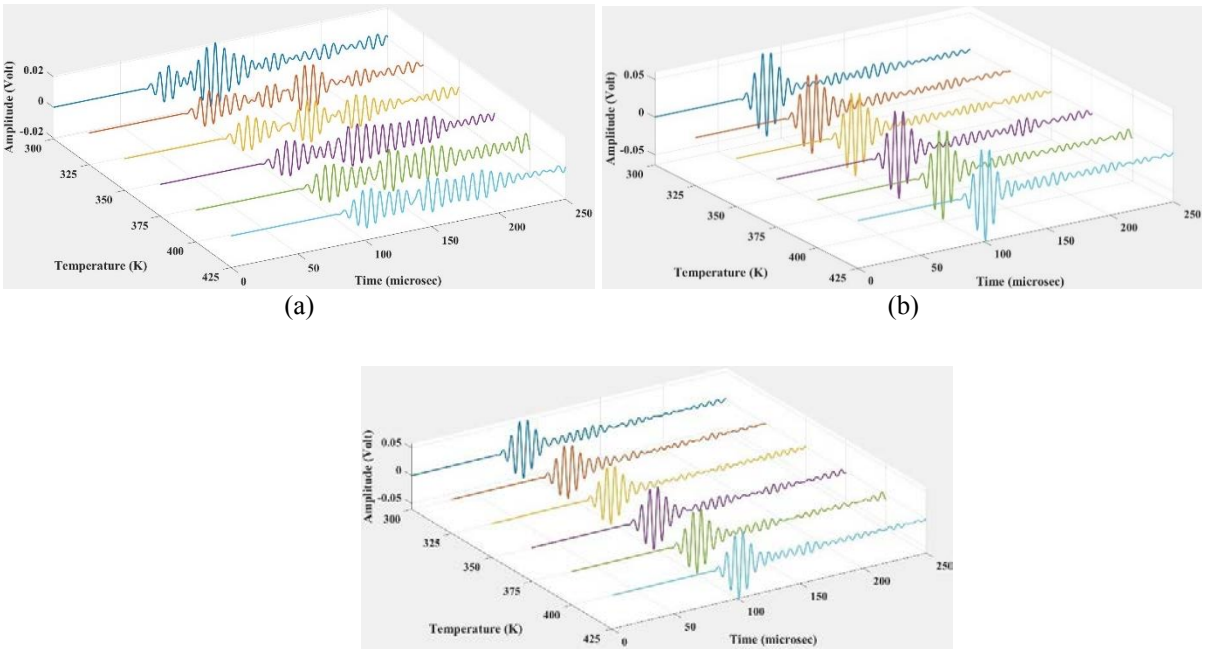

Figure 16: Response obtained at P5 for different intensities of temperature exposure in the panel with debond size of (a) δ= 0 mm, (b) δ= 25 mm and (c) δ= 50 mm.

Furthermore, the investigation is being carried out to examine the variation of the CWT peak and group velocity of the S0 mode of the wave under the influence of temperature for different debonding lengths. Fig. 18 (a) depicts a gradual enhancement in the magnitude of the CWT peak of S0 mode with the temperature rise. However, the magnitude of the CWT peak increases significantly in the presence of debonding. On the other hand, the magnitude of the wavelet peak of A0 mode drops initially with a slight rise in the temperature and further enhances with the increase in temperature. Further, at a higher temperature intensity, the CWT peak drops in the bonded panel. Apart from this, the group velocity of the S0 mode reduces gradually as the temperature is increased, regardless of the debonded length. However, at the reference temperature, a quite noticeable drop is noticed in the velocity with debonding. At the higher temperature, the group velocity of the S0 mode in the debonded panel is slightly higher than the bonded panel S0 mode group velocity, as observed in Fig. 18 (b).

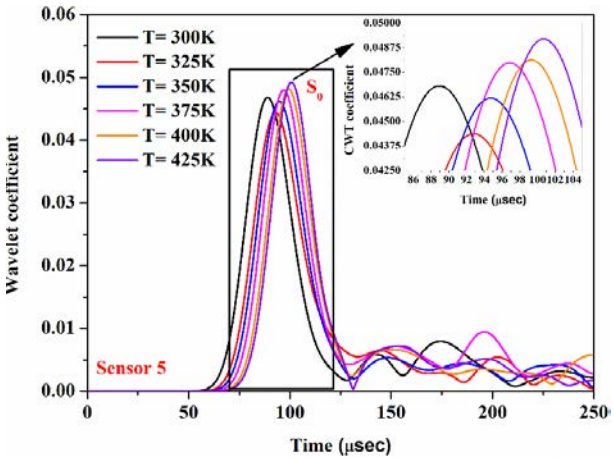

Figure 17: CWT of the P5 sensor signal obtained at 150 kHz for the panel with δ= 25 mm.

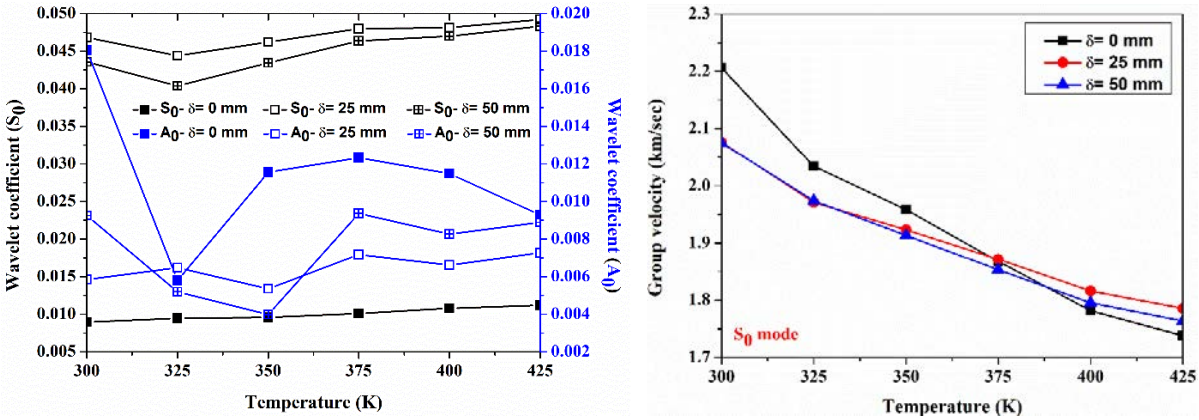

Figure 18: Influence of the thermal variation on the (a) CWT of the response (b) group velocity of the S0 mode of the wave obtained at P5.

4.3.4 Influence of moisture concentration on the scattered GW response for different debonding length

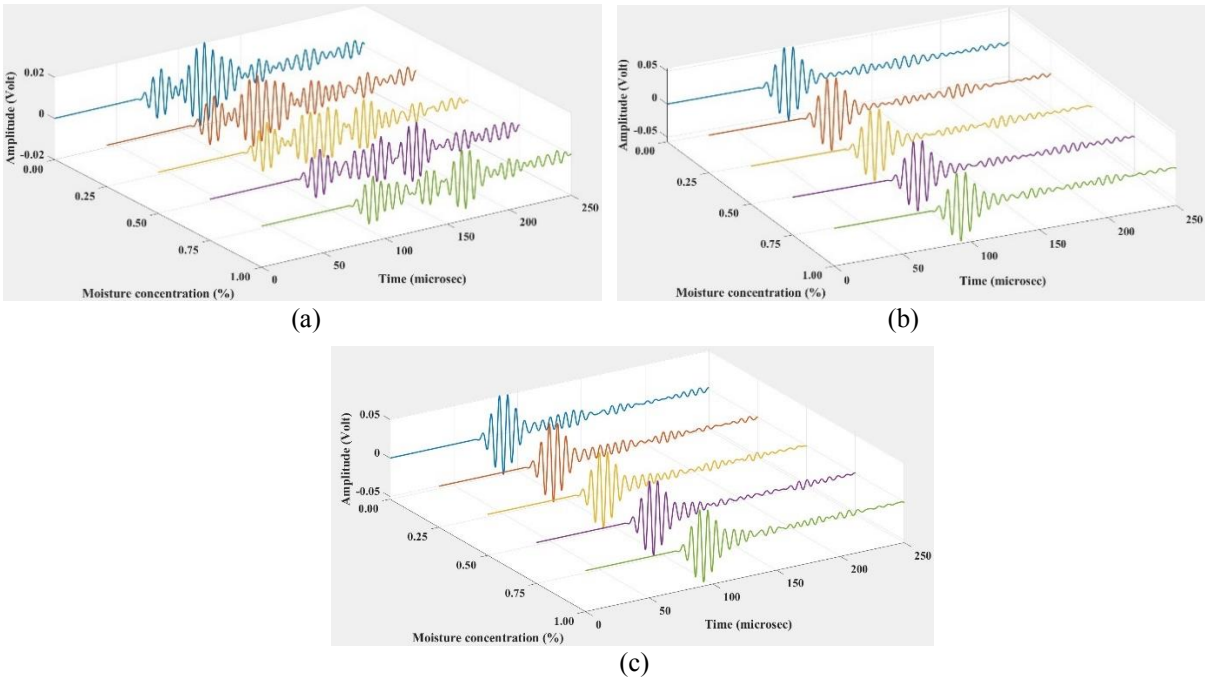

Figure 19: Response obtained at P5 for different moisture concentrations in the panel with debond size of (a) δ= 0 mm, (b) δ= 25 mm and (c) δ= 50 mm.

This section discusses the study conducted to comprehend the influence of moisture concentration on the scattered guided wave's response for different debonding lengths. Similar to the thermal variation, uniform moisture is exposed on the panel. Apart from this moisture dependent material properties are used for the composite structure. As no works of literature are available on the variation of moisture concentration on the piezoelectric material properties, therefore, the piezo properties are maintained constant throughout the study. The stability study showed that the panel buckles at a moisture concentration of 1.1427%, 1.1422% and 1.1401% for a bonded panel, 25 mm debonded panel, and 50 mm debonded panel. Hence, the current study is conducted by varying the moisture from 0.0% to 1.0% at an interval of 0.25%. The response of the wave obtained at P5 is shown in Fig. 19 for various lengths of

debonding. The plot shows that the time range of the S0 mode packet slightly broadens as the moisture concentration rises for a larger debond length. However, with debonding, the amplitude of the S0 mode response increases significantly. On the other hand, contrary behaviour is noticed in the case of A0 mode. The amplitude of the mode reduces tremendously and narrows down the A0 wave packet propagating length with the enhancement in the moisture concentration. It is interesting to notice that with debonding, the S0 mode travels with a higher amplitude, whereas the A0 mode amplitude reduces.

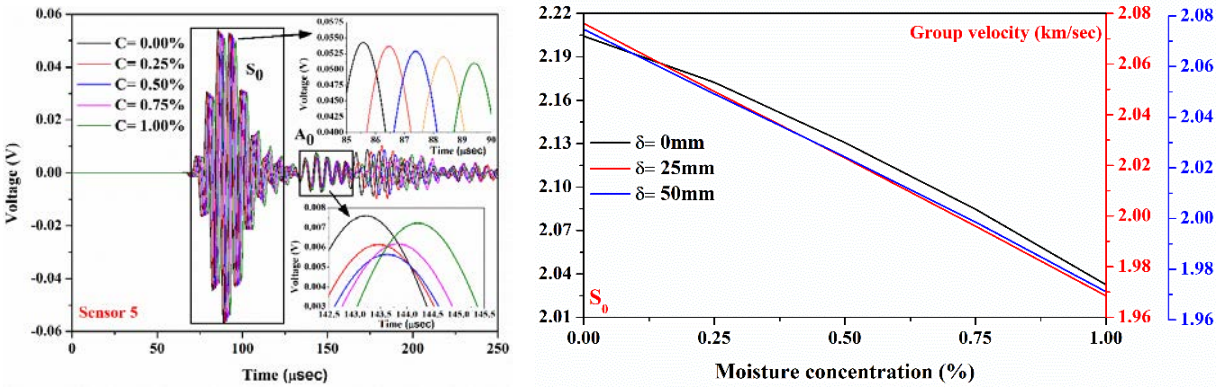

(a) (b)

Figure 20: (a) Response obtained at the P5 sensor signal in the panel with δ= 25 mm, (b) Influence of moisture concentration on the group velocity of the S0 mode for different debonding sizes.

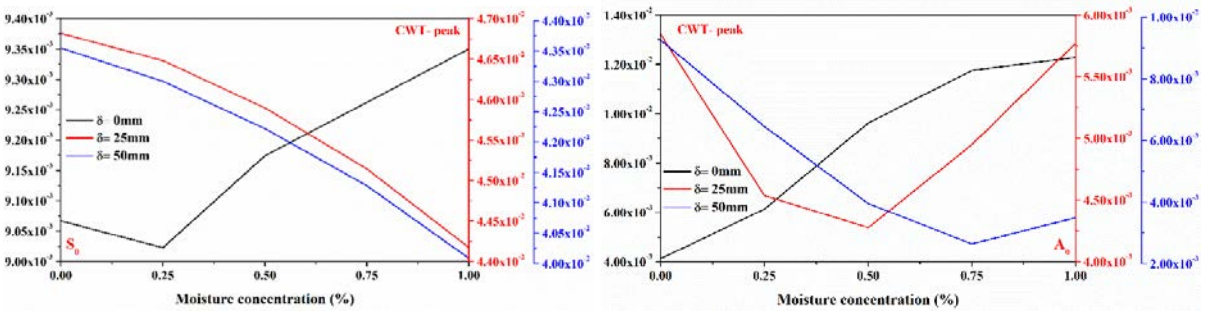

(a) (b)

Figure 21: Variations of the magnitude of the CWT peak for (a) S0 mode and (b) A0 mode for different sizes of debonding.

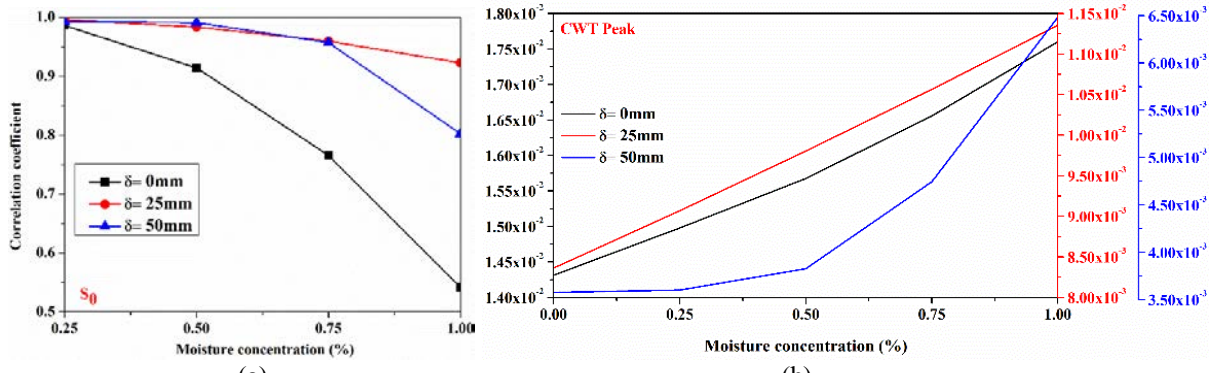

(a) (b)

Figure 22: Influence of moisture concentration on (a) correlation coefficient of the response obtained at P5 and (b) magnitude of the CWT peak of the S0 mode response captured at P8 for different debonding lengths.

Fig. 20 (a) shows the 25 mm debonded panel response obtained at P5 for different moisture concentration exposure. It is observed that similar to the loading influence, the moisture mar-

ginally influences the wave response of the panel. The amplitude of the S0 mode reduces gradually with some delay in the arrival of the mode. This shows the reduction in the group velocity of the wave mode with the rise in the moisture concentration. On the other hand, the amplitude of the A0 mode decreases with the initial exposure to low moisture concentration, and at higher moisture concentration, the amplitude enhances with the rise in the moisture concentration along with the delay in the arrival of the packet, indicating the reduction in the group velocity. Fig. 20 (b) depicts the variation in S0 mode group velocity in the transverse direction of the plies for various debonding lengths. Here, it is observed that moisture noticeably reduces the wave's group velocity with the increase in the moisture concentration, irrespective of the debonding size. However, a sudden drop in the wave's group velocity occurs with the introduction of debonding. Further increase in the debond marginally reduces the group velocity.

The influence of the moisture concentration on the magnitude of the CWT peak of the S0 and A0 wave modes for different debonding sizes is presented in Fig. 21. The plot shows that the magnitude of the CWT peak of the S0 mode in the bonded panel response initially reduces with the introduction of moisture, and then it increases with the moisture concentration. However, as the debonding size increases, the peak's magnitude decreases with moisture concentration. On the other hand, the magnitude of the CWT peak of the A0 mode in the bonded panel increases as the moisture concentration increases. The CWT peak of the A0 mode in the debonded panel initially drops and then increases with increasing moisture concentration. As the debonding increase, the peak drops for higher moisture concentration.

From Fig. 22 (a), it is noted that the correlation coefficient of the scattered wave reduces with the increases in the moisture concentration. However, the debonded panel signal features change slightly as the moisture concentration increases in comparison to the signal in the panel subjected to 0% moisture. This demonstrates that the wave features in a bonded panel change more abruptly as a result of moisture exposure than the wave features in a debonded panel.

Fig. 22 (b) highlights the variation of the CWT peak of the first packet in the response obtained at the P8 sensor, which is attached to the top surface of the stiffener flange right above the debond. According to the findings, the CWT peak increases linearly with the rise in the moisture concentration in the bonded panel. However, as the debonding size increases, the CWT peak enhancement exhibits a parabolic variation. Aside from that, the magnitude of the CWT peak decreases with debonding propagation.

5 CONCLUDING REMARKS

The current research investigates the impact of environmental and loading factors on the GW response of an interfacial debonded stiffened panel while accounting for residual stress developed by hygrothermal load and in-plane load. Numerical modelling with multiphysics coupling has been developed using finite element simulation software "COMSOL Multiphysics". Apart from numerical modelling, the scattered signals are processed to understand the variation of different wave features under the influence of hygrothermal and external loading conditions. Detailed numerical investigations of the scattered response obtained from the simulation are performed to investigate the external loading and environmental effect. Based on the results obtained from this investigation, the following conclusion can be reached:

i. Based on the frequency modulation study, the 5-cycle Hanning window excited with 150 kHz frequency has better A0 and S0 mode scattered response and is used as excitation frequency for the other parametric studies.

ii. In the case of the bonded panel, the response signal has a high A0 mode amplitude and a smaller S0 mode amplitude. However, a contrary behaviour is noticed in the debonded panel, as the scattered wave will have a high S0 mode amplitude and a smaller A0 mode amplitude.
iii. The amplitude of the A0 mode of the scattered GW response reduces as the debonding size increases, which contradicts the behaviour of the S0 mode.
iv. The amplitude of the scattered S0 mode GW response captured by the attached PZT enhances as the debonding length increases. However, the amplitude of the S0 mode obtained using PZT bonded on the stiffener flange reduces as the debonding length increases.
v. Inplane load marginally affects the response of the scattered wave. However, the peak of the S0 and A0 modes reduces with the increase in the magnitude of the compressive edge loading.
vi. The group velocity of the A0 mode drops with the enhancement in the intensity of compressive edge load, but it is insignificant in the case of the S0 mode.
vii. The CWT peak of the S0 and A0 modes increases as the applied in-plane pressure enhances. However, a slight drop in the peak is observed in the case of a 50 mm debonded panel response.
viii. Similar to the external in-plane load, the temperature reduces the group velocity of the S0 mode.
ix. The amplitude of the S0 mode initially reduces with the rise in the moisture concentration for the bonded panel. In the case of a debonded panel, the wave amplitude reduces parabolically with the moisture concentration.
x. The time drift of the S0 mode packet of the response in the bonded panel reduces significantly. However, it widens as the debonded length increases.
xi. The time length of the A0 mode of the response reduces with the increase in the moisture concentration in the panel. However, the amplitude analogously reduces, as observed in the other loading case.

The above findings show that the hygrothermal loading significantly influences the scattered wave response more than the applied in-plane pressure. Therefore, this study can be used as a reference investigation to apprehend the influence of the complex loading conditions on the guided wave response.

REFERENCES

[1] J. Guo, X. Gao, E. Toma, U. Netzelmann, Anisotropy in carbon fiber reinforced polymer (CFRP) and its effect on induction thermography, *NDT & E International.* **91** 1-8, 2017.
[2] M.F. Haider, M.M. Haider, F. Yasmeen, Micromechanics model for predicting anisotropic electrical conductivity of carbon fiber composite materials, *AIP Conference Proceedings.* **1754 (1),** 030011, 2016.
[3] C. Meola, S. Boccardi, G.M. Carlomagno, Composite material overview and its testing for aerospace components, in: M. Jawaid, M. Thariq (Eds.) Sustainable Composites for Aerospace Applications, Woodhead Publishing, 2018, pp. 69-108.
[4] X. Zhang, X. Wu, Y. He, S. Yang, S. Chen, S. Zhang, D. Zhou, CFRP barely visible impact damage inspection based on an ultrasound wave distortion indicator, *Composites Part B: Engineering.* **168** 152-158, 2019.

[5] B. Park, Y.-K. An, H. Sohn, Visualization of hidden delamination and debonding in composites through noncontact laser ultrasonic scanning, *Composites Science and Technology.* **100** 10-18, 2014.
[6] L. Ye, Z. Su, Identification of damage using Lamb waves, *J Lecture notes in applied computational mechanics.* **48** 4-5, 2009.
[7] J.-R. Lee, J. Takatsubo, N. Toyama, Disbond monitoring at wing stringer tip based on built-in ultrasonic transducers and a pulsed laser, *Smart Materials and Structures.* **16 (4),** 1025-1035, 2007.
[8] G.A.O. Davies, D. Hitchings, J. Ankersen, Predicting delamination and debonding in modern aerospace composite structures, *Composites Science and Technology.* **66 (6),** 846-854, 2006.
[9] H. Sohn, D. Dutta, J.Y. Yang, M. DeSimio, S. Olson, E. Swenson, Automated detection of delamination and disbond from wavefield images obtained using a scanning laser vibrometer, *Smart Materials and Structures.* **20 (4),** 045017, 2011.
[10] R. Seydel, F.-K. Chang, Impact identification of stiffened composite panels: I. System development, *Smart Materials and Structures.* **10 (2),** 354-369, 2001.
[11] J.L. Rose, Ultrasonic waves in solid media, in, Acoustical Society of America, 2000.
[12] N. Guo, P. Cawley, The interaction of Lamb waves with delaminations in composite laminates, *The Journal of the Acoustical Society of America.* **94 (4),** 2240-2246, 1993.
[13] M.J.S. Lowe, R.E. Challis, C.W. Chan, The transmission of Lamb waves across adhesively bonded lap joints, *The Journal of the Acoustical Society of America.* **107 (3),** 1333-1345, 2000.
[14] C. Ramadas, K. Balasubramaniam, M. Joshi, C.V. Krishnamurthy, Interaction of Lamb mode (Ao) with structural discontinuity and generation of "Turning modes" in a T-joint, *Ultrasonics.* **51 (5),** 586-595, 2011.
[15] C. Han, G. Yang, J. Wang, X. Guo, The research on propagation characteristics of acoustic emission signals in stiffened plates based on the multipath propagation model, *Ultrasonics.* **108** 106177, 2020.
[16] F. Chen, P.D. Wilcox, The effect of load on guided wave propagation, *Ultrasonics.* **47 (1),** 111-122, 2007.
[17] S.J. Lee, N. Gandhi, J.E. Michaels, T.E. Michaels, Comparison of the effects of applied loads and temperature variations on guided wave propagation, in: AIP Conference Proceedings, American Institute of Physics, 2011, pp. 175-182.
[18] J.E. Michaels, S.J. Lee, T.E. Michaels, Impact of applied loads on guided wave structural health monitoring, in: AIP Conference Proceedings, American Institute of Physics, 2011, pp. 1515-1522.
[19] S. Roy, P. Ladpli, F.-K. Chang, Load monitoring and compensation strategies for guided-waves based structural health monitoring using piezoelectric transducers, *Journal of Sound and Vibration.* **351** 206-220, 2015.
[20] R. Radecki, W.J. Staszewski, T. Uhl, Impact of Changing Temperature on Lamb Wave Propagation for Damage Detection, *Key Engineering Materials.* **588** 140-148, 2014.
[21] M.J. Boon, D. Zarouchas, M. Martinez, D. Gagar, B. Rinze, P. Foote, Temperature and load effects on acoustic emission signals for structural health monitoring applications, in: EWSHM-7th European Workshop on Structural Health Monitoring, 2014.
[22] S. Roy, K. Lonkar, V. Janapati, F.-K. Chang, A novel physics-based temperature compensation model for structural health monitoring using ultrasonic guided waves, *J Structural Health Monitoring.* **13 (3),** 321-342, 2014.

[23] S. Sikdar, P. Fiborek, P. Kudela, S. Banerjee, W. Ostachowicz, Effects of debonding on Lamb wave propagation in a bonded composite structure under variable temperature conditions, *Smart Materials and Structures.* **28 (1),** 015021, 2018.
[24] C.A. Dan, P. Kudela, M. Radzienski, W. Ostachowicz, Temperature effects compensation strategy for guided wave based structural health monitoring, in: 6th International Symposium on NDT in Aerospace, Madrid, Spain, 2014.
[25] K.J. Schubert, A.S. Herrmann, On the influence of moisture absorption on Lamb wave propagation and measurements in viscoelastic CFRP using surface applied piezoelectric sensors, *Composite Structures.* **94 (12),** 3635-3643, 2012.
[26] K. Lonkar, Modeling of piezo-induced ultrasonic wave propagation for structural health monitoring Stanford, in, PhD Thesis, 2013.
[27] L. Qiu, R.S. Venkat, C. Boller, S. Yuan, Multiphysics Simulation of Guided Wave Propagation under Load Condition, in: 8th Internat. Symp. on NDT in Aerospace, 2016.
[28] P.K. Parhi, S.K. Bhattacharyya, P.K. Sinha, Hygrothermal effects on the dynamic behavior of multiple delaminated composite plates and shells, *Journal of Sound and Vibration.* **248 (2),** 195-214, 2001.
[29] C. Bijudas, M. Mitra, P. Mujumdar, Time reversed Lamb wave for damage detection in a stiffened aluminum plate, *J Smart materials structures.* **22 (10),** 105026, 2013.
[30] A.P. Kalgutkar, S. Banerjee, Semi-Analytical Finite Element Method for the Analysis of Guided Wave Dispersion in the Pre-stressed Composite Plates, *ASPS Conference Proceedings.* **1 (5),** 1413-1421, 2022.